



TITLE:

# Intrafractional tracking accuracy in infrared marker-based hybrid dynamic tumour-tracking irradiation with a gimballed linac.

AUTHOR(S):

Mukumoto, Nobutaka; Nakamura, Mitsuhiro; Yamada, Masahiro; Takahashi, Kunio; Tanabe, Hiroaki; Yano, Shinsuke; Miyabe, Yuki; ... Sawada, Akira; Kokubo, Masaki; Hiraoka, Masahiro

---

CITATION:

Mukumoto, Nobutaka ...[et al]. Intrafractional tracking accuracy in infrared marker-based hybrid dynamic tumour-tracking irradiation with a gimballed linac.. Radiotherapy and oncology : journal of the European Society for Therapeutic Radiology and Oncology 2014, 111(2): 301-305

ISSUE DATE:

2014-05

URL:

<http://hdl.handle.net/2433/188903>

RIGHT:

© 2014 Elsevier Ireland Ltd.; This is not the published version. Please cite only the published version.; この論文は出版社版ではありません。引用の際には出版社版をご確認ご利用ください。

## Intrafractional accuracy of IR Tracking

# 1 Intrafractional tracking accuracy in infrared marker-based hybrid 2 dynamic tumour-tracking irradiation with a gimballed linac

3

4 Nobutaka Mukumoto<sup>a</sup>, Mitsuhiro Nakamura<sup>a,\*</sup>, Masahiro Yamada<sup>a</sup>, Kunio  
5 Takahashi<sup>b</sup>, Hiroaki Tanabe<sup>c</sup>, Shinsuke Yano<sup>d</sup>, Yuki Miyabe<sup>a</sup>, Nami Ueki<sup>a</sup>, Shuji  
6 Kaneko<sup>a</sup>, Yukinori Matsuo<sup>a</sup>, Takashi Mizowaki<sup>a</sup>, Akira Sawada<sup>a,e</sup>, Masaki Kokubo<sup>c,f</sup>,  
7 and Masahiro Hiraoka<sup>a</sup>

8 <sup>a</sup> Department of Radiation Oncology and Image-applied Therapy, Graduate School of  
9 Medicine, Kyoto University, Kyoto, Japan

10 <sup>b</sup> Advanced Mechanical Systems Department, Mitsubishi Heavy Industries Ltd, Hiroshima,  
11 Japan

12 <sup>c</sup> Division of Radiation Oncology, Institute of Biomedical Research and Innovation, Hyogo,  
13 Japan

14 <sup>d</sup> Division of Clinical Radiology Service, Kyoto University Hospital, Kyoto, Japan

15 <sup>e</sup> Department of Radiological Technology, Faculty of Medical Science, Kyoto College of  
16 Medical Science, Kyoto, Japan

17 <sup>f</sup> Department of Radiation Oncology, Kobe City Medical Center General Hospital, Hyogo,  
18 Japan

19

20 \* **Corresponding author:** Mitsuhiro Nakamura, Ph.D., Graduate School of Medicine,  
21 Kyoto University, 54 Kawahara-cho, Shogoin, Sakyo-ku, Kyoto, 606-8507, Japan.

22 Tel.: +81-75-751-3762; Fax: +81-75-771-9749; E-mail: [m\\_nkmr@kuhp.kyoto-u.ac.jp](mailto:m_nkmr@kuhp.kyoto-u.ac.jp)

## Intrafractional accuracy of IR Tracking

23

24 Total number of pages: 16 (**Tables: 2; Figures: 2; Supplementary Material: 1**)

25

26 **Running title:** Intrafractional accuracy of IR Tracking

27

28 **Key words:** Four-dimensional image-guided radiotherapy, dynamic tumour-tracking  
29 irradiation, respiratory motion, Vero4DRT, intra-fractional tracking accuracy.

30

31 **Meeting presentation:** This work was accepted for presentation during the poster viewing  
32 session of the 54<sup>th</sup> Annual Meeting of the American Society for Radiation Oncology in  
33 Boston, October 28-31, 2012.

34

## Intrafractional accuracy of IR Tracking

### ABSTRACT

**Purpose:** To verify the intrafractional tracking accuracy in infrared (IR) marker-based hybrid dynamic tumour tracking irradiation (“IR Tracking”) with the Vero4DRT.

**Materials and Methods:** The gimballed x-ray head tracks a moving target by predicting its future position from displacements of IR markers in real-time. Ten lung cancer patients who underwent IR Tracking were enrolled. The 95<sup>th</sup> percentiles of intrafractional mechanical ( $iE_M^{95}$ ), prediction ( $iE_P^{95}$ ), and overall targeting errors ( $iE_T^{95}$ ) were calculated from orthogonal fluoroscopy images acquired during tracking irradiation and from the synchronously acquired log files.

**Results:** Averaged intrafractional errors were (left-right, cranio-caudal [CC], anterior-posterior [AP]) = (0.1 mm, 0.4 mm, 0.1 mm) for  $iE_M^{95}$ , (1.2 mm, 2.7 mm, 2.1 mm) for  $iE_P^{95}$ , and (1.3 mm, 2.4 mm, 1.4 mm) for  $iE_T^{95}$ . By correcting systematic prediction errors in the previous field, the  $iE_P^{95}$  was reduced significantly, by an average of 0.4 mm in the CC ( $p < 0.05$ ) and by 0.3 mm in the AP ( $p < 0.01$ ) directions.

**Conclusions:** Prediction errors were the primary cause of overall targeting errors, whereas mechanical errors were negligible. Furthermore, improvement of the prediction accuracy could be achieved by correcting systematic prediction errors in the previous field.



## Intrafractional accuracy of IR Tracking

53

**INTRODUCTION**

54 Respiratory motion is one of the factors causing uncertainties during beam delivery,  
55 particularly for thoracic and abdominal tumours [1, 2]. In hypofractionated stereotactic  
56 body radiotherapy for lung cancer patients, addition of a large margin to compensate for  
57 respiratory motion increases the probability of complications [3]. Several techniques,  
58 including forced shallow-breathing, breath-hold, respiratory gating, and dynamic tumour  
59 tracking (DTT), have been proposed to reduce the uncertainties caused by respiratory  
60 motion [1, 2]. Of these methods, recent interest has focused on the DTT technique, which  
61 can reposition the radiation beam dynamically in accordance with the target position. DTT  
62 can minimise the internal uncertainties without a burden on the respiration of patients or  
63 prolongation of treatment time.

64 We have developed an innovative four-dimensional (4D) image-guided  
65 radiotherapy system, the Vero4DRT (MHI-TM2000; Mitsubishi Heavy Industries, Ltd.,  
66 Japan, and BrainLAB, Feldkirchen, Germany) [4-10], and used its hybrid DTT irradiation  
67 function [infrared (IR)-marker-based hybrid DTT irradiation (“IR Tracking”)] clinically in  
68 lung cancer patients since September 2011 [10]. In IR Tracking, the position of the target,  
69 indicated by implanted fiducial markers, is calculated from external surrogate signals  
70 through a pre-built prediction model (“4D model”), and the MV x-ray beam is delivered  
71 with real-time monitoring [7, 8, 10-12]. Depuydt et al. showed that the performance of  
72 Vero4DRT’s DTT function was comparable with other clinical DTT systems in phantom  
73 and patient simulation studies [11, 12]. Our group also previously revealed that the  
74 accuracy of the 4D model must be verified before treatment, and margins were required to

## Intrafractional accuracy of IR Tracking

compensate for the prediction error in a phantom study [7]; it was concluded that the accuracy of the 4D model was affected by the baseline drift of respiratory motion [8]. Here, we verified the intrafractional tracking accuracy of IR Tracking for lung cancer patients using intrafractional monitoring images and the corresponding log files.

## MATERIALS AND METHODS

### *The Vero4DRT hybrid dynamic tumour tracking irradiation system*

Supplementary Figure 1 (Electronic Appendix) shows a schematic diagram of the Vero4DRT system. The Vero4DRT has several unique components that facilitate DTT irradiation: (1) a compact C-band 6-MV x-ray head with a gimbal mechanism, mounted on an O-ring gantry. The gimballed x-ray head can swing itself in both the pan and tilt directions, (2) gantry-mounted orthogonal kV x-ray imaging subsystems, consisting of two sets of x-ray tubes and flat-panel detectors, with a spatial resolution of 0.2 mm at the isocentre level, and (3) an extended version of the ExacTRAC system that enables real-time motion monitoring and management for the DTT function [7, 8, 11, 12] with an IR camera mounted on the ceiling of the treatment room.

Supplementary Figure 2 shows a schematic diagram of the IR Tracking procedure. After patient positioning, a 4D model is created using synchronously monitored internal target motion and an external surrogate signal. The detected target position ( $P_d$ ) is defined as the tumour centre-of-mass calculated from the positions of the implanted fiducial markers on the x-ray images. The relative shift amount between the tumour centre-of-mass and centroid of the markers' polyhedron was determined at the end-exhalation phase in the

## Intrafractional accuracy of IR Tracking

planning computed tomography. The predicted target position ( $P_p$ ) is calculated from the 4D model, expressed by a quadratic equation involving two variables, the position and velocity of the IR markers. The positions of the IR markers are predicted linearly from the past motion to compensate for the DTT system delay [11]. Details of the prediction model are described in the Supplementary Materials section. In this 4D-modelling phase, the peak-to-peak amplitude of the detected target motion ( $A$ ) and the mean ( $\mu$ ) and standard deviation ( $SD$ ) of the absolute 4D-modelling error ( $E_{4DM}$ ), defined as the absolute difference between the  $P_p$  and  $P_d$ , are calculated along each axis automatically. During beam delivery, the future 3D target position is calculated from the displacements of the IR markers using the 4D model, and then the corresponding tracking angle is transferred continuously to the gimballed x-ray head. Additionally, circles with a user-defined radius around the predicted positions of the fiducial markers (tolerance circles) are displayed on the monitoring images as a benchmark in re-modelling. When the fiducial markers are deviated systematically from the tolerance circles, re-modelling should be performed during each treatment session (Fig. 1).

### ***Patient characteristics and treatment planning***

Ten lung cancer patients who underwent IR Tracking in an Institutional Review Board-approved trial were included in the present study. Patient selection criteria were based on our stereotactic body radiation therapy protocol and written informed consent for the present study was obtained from each patient [3, 10]. Three or more 1.5-mm-diameter gold markers (Olympus Co., Tokyo, Japan) were implanted around the lung tumour

## Intrafractional accuracy of IR Tracking

transbronchially 1–2 weeks before treatment planning. Table 1 shows the characteristics of the patients and treatment planning. We performed a dry-run treatment session prior to treatment planning to assess the characteristics of respirations and to identify patient-specific planning target volume (PTV) margins [7, 9]. The median of  $A$  was 2.8 mm in the left-right (LR), 15.8 mm in the cranio-caudal (CC), and 4.3 mm in the anterior-posterior (AP) directions. The median of  $\mu+2SD$  of the  $E_{4DM}$  during the dry-run treatment session ( $E_{4DM}^{\mu+2SD}$ ) was 0.6 mm in the LR, 1.9 mm in the CC, and 0.7 mm in the AP directions. Patient-specific PTV margins of 5.0–9.0 mm were added to the tumour along each axis to compensate for intra- and interfractional uncertainties in IR Tracking [7, 9, 13]. Supplementary Figure 3 shows the definition of the patient-specific PTV margins. The intra- and interfractional uncertainties were classified into systematic and random components. The patient-specific PTV margins were then calculated for each axis using the formula in Supplementary Figure 3. Prescribed doses of 48 or 56 Gy were specified to isocentre in four fractions. Treatment plans included 6-8 non-coplanar fields, with a dose rate of 500 MU/min.

### ***Data acquisition during beam delivery***

During beam delivery, the target and fiducial markers were monitored using orthogonal kV x-ray imaging subsystems at 1 Hz. The predicted target positions and tracking angles of the gimballed x-ray head were recorded in log files at 60 and 200 Hz, respectively. In total, 9268 paired images (~30 paired images per field) and corresponding log files were acquired.

## Intrafractional accuracy of IR Tracking

141

142 ***Verification of intrafractional tracking accuracy***

143 Intrafractional tracking accuracy was verified by the  $P_d$  from the fluoroscopic images and  
144 the corresponding  $P_p$  and the tracked target position, calculated from the synchronously  
145 acquired log files. Supplementary Figure 4 shows the geometric point of the tracked target  
146 position at the depth of the  $P_d$  ( $P_{t,d}$ ). The tracked target position at the depth of the  $P_p$  ( $P_{t,p}$ ),  
147 was calculated similarly. Intrafractional mechanical ( $iE_M$ ), prediction ( $iE_P$ ), and overall  
148 targeting errors ( $iE_T$ ) were defined as the differences between  $P_{t,p}$  and  $P_p$ ,  $P_p$  and  $P_d$ , and  $P_{t,d}$   
149 and  $P_d$ , respectively. Details of the calculation process are described in the Supplementary  
150 Materials section.

151 The 95<sup>th</sup> percentiles of the absolute  $iE_M$  ( $iE_M^{95}$ ),  $iE_P$  ( $iE_P^{95}$ ), and  $iE_T$  ( $iE_T^{95}$ ) during  
152 the treatment course were then calculated using the intrafractional monitoring images and  
153 the corresponding log files. Pearson correlation coefficients were calculated to assess the  
154 relationship between  $E_{4DM}^{\mu+2SD}$  during the dry-run treatment session and  $iE_P^{95}$  or  $iE_T^{95}$   
155 during the treatment course. To further improve the prediction accuracy, the corrected  $iE_P^{95}$   
156 was recalculated retrospectively by subtracting the systematic (*i.e.* signed overall mean)  $iE_P$   
157 in the previous field excluding the first field after the 4D modelling. A paired *t*-test with a  
158 0.05 significance level was performed for statistical analysis.

## RESULTS

161 Table 2 summarises  $iE_M^{95}$ ,  $iE_P^{95}$ ,  $iE_T^{95}$ , and corrected  $iE_P^{95}$  for 10 lung cancer patients.

## Intrafractional accuracy of IR Tracking

162 Averaged intrafractional tracking errors were (LR, CC, AP) = (0.1 mm, 0.4 mm, 0.1 mm)  
163 for  $iE_M^{95}$ , (1.2 mm, 2.7 mm, 2.1 mm) for  $iE_P^{95}$ , and (1.3 mm, 2.4 mm, 1.4 mm) for  $iE_T^{95}$ .  
164 Additionally, a strong positive correlation was found between  $E_{4DM}^{\mu+2SD}$  and  $iE_P^{95}$  (LR, CC,  
165 AP) = (0.73 [ $p = 0.017$ ], 0.82 [ $p = 0.003$ ], 0.96 [ $p = 0.000$ ]) or  $iE_T^{95}$  (LR, CC, AP) = (0.69  
166 [ $p = 0.028$ ], 0.77 [ $p = 0.010$ ], 0.90 [ $p = 0.001$ ]). As shown in Table 2,  $iE_P^{95}$  was the  
167 primary cause of  $iE_T^{95}$ , while  $iE_M^{95}$  was negligible. The  $iE_T^{95}$  was fully covered by the  
168 PTV margin, including the geometric variations between the tumour and fiducial markers.  
169 Figure 2 (a) shows representative probability histograms in the positional error in the CC  
170 direction for the first patient who underwent IR Tracking (Patient No. 1).  $iE_T^{95}$  was  
171 2.3 mm for this patient.

172 A maximum  $iE_T^{95}$  of 4.1 mm was observed for Patient No. 7 in the CC direction.  
173 This patient showed the largest difference between  $E_{4DM}^{\mu+2SD}$  and  $iE_P^{95}$  [LR, CC, and AP =  
174 1.6, 1.5, and 1.6 mm, respectively] due to a baseline drift during beam delivery. Meanwhile,  
175 the averaged differences for the other patients were 0.3, 0.6, and 0.7 mm for the LR, CC,  
176 and AP directions, respectively. By correcting the systematic prediction errors in the  
177 previous field, however,  $iE_P^{95}$  decreased, from 4.1 to 2.7 mm, for this patient in the CC  
178 direction [Fig. 2 (b)]. The maximum reductions in  $iE_P^{95}$  were observed in this patient (LR,  
179 CC, AP) = (1.4 mm, 1.4 mm, 0.9 mm). For the entire population, the corrected  $iE_P^{95}$  was  
180 improved significantly by an average of 0.4 mm in the CC ( $p < 0.05$ ) and by 0.3 mm in the  
181 AP ( $p < 0.01$ ) directions.

## Intrafractional accuracy of IR Tracking

182

183

### DISCUSSION

184 The Vero4DRT tracks a moving target in real-time using the orthogonal gimballed x-ray  
185 head. In the present study, we established a verification methodology for the intrafractional  
186 mechanical, prediction, and overall targeting accuracy in each axis during the treatment  
187 course. The 3D coordinates of the intrafractional tracked target position were calculated  
188 based on the MV x-ray beam orientation using intrafractional monitoring images and the  
189 corresponding log files.

190 We verified the intrafractional tracking accuracy for 10 lung cancer patients who  
191 underwent IR Tracking with real-time monitoring. Vero4DRT users can monitor the moving  
192 target, fiducial markers, and tolerance circles with its predicted position using orthogonal  
193 kV x-ray imaging subsystems during beam delivery. At our institution, the radius of the  
194 tolerance circles is set to 3 mm, and the 4D model is re-modelled when the monitored  
195 fiducial markers' positions are displaced systematically from the tolerance circles due to  
196 baseline drift (Fig. 1). By re-modelling the 4D model, while an  $iE_T^{95}$  of less than 3 mm  
197 was achieved for nine patients (90%), one patient (Patient No. 7) showed a large  $iE_T^{95}$  of  
198 greater than 3 mm. The 4D model was updated once during the treatment session for  
199 Patient No. 7. However, this patient required additional re-modelling. In IR Tracking, the  
200 predominant cause of overall targeting errors was prediction errors. The position and  
201 velocity of IR markers involved in the 4D model were predicted linearly from past IR  
202 marker motion [8]. Thus, prediction uncertainty of the peak position sometimes  
203 overestimated the predicted position of the IR marker and the 4D model enforced a large

## Intrafractional accuracy of IR Tracking

204 amplitude of respiration motion (Supplementary Figure 5). In this case, the mechanical  
205 response delay of the gimballed x-ray head reduced the impact of the prediction error on  
206 the overall targeting error. Thus, the overall targeting errors were sometimes smaller than  
207 the prediction errors. Additionally, there were strong correlations between  $E_{4DM}^{\mu+2SD}$  and  
208  $iE_p^{95}$  or  $iE_T^{95}$ , indicating that intrafractional prediction or overall targeting errors during  
209 the treatment course could be estimated from 4D modelling errors during the dry-run  
210 treatment session. The  $iE_T^{95}$  was fully covered by the PTV margin, including a geometric  
211 variation between the tumour and fiducial markers of 2.5 mm (Tables 1 and 2). When  
212 calculating the PTV margin in IR Tracking, the intra- and interfractional uncertainties  
213 should be considered (Supplementary Figure 3). However, the present recipe of the  
214 patient-specific PTV margin was tentative so as to perform IR Tracking safely. Therefore,  
215 further investigations will be needed to determine the PTV margin size appropriate for IR  
216 Tracking [9].

217 The CyberKnife Robotic Radiosurgery System with the integrated Synchrony  
218 Respiratory Tracking System (Accuray, Sunnyvale, CA) substantially reduces the  
219 geometric error caused by respiratory motion [14, 15]. In the present study,  $E_{4DM}^{\mu+2SD}$  was  
220 comparable with results of the Synchrony system. However, the correlation between the  
221 internal target positions and external surrogates can change in the presence of baseline drift,  
222 reducing the accuracy of the prediction model [8, 16]. The Synchrony system periodically  
223 updates the prediction model using the intrafractional monitoring images. Updating the 4D  
224 model in real-time may also improve the prediction accuracy because the internal/external



## Intrafractional accuracy of IR Tracking

correlation change or baseline drift in respiration will be corrected. Meanwhile, this is difficult regarding image processing time and minimum interval of the x-ray acquisition during beam delivery. The 4D model in IR Tracking includes the parameters of position and velocity of the IR markers. To update the 4D model, these parameters must be changed. Thus, a shorter monitoring interval would be necessary. In clinical practice, we re-modelled the 4D model at least once during treatment to minimise intrafractional uncertainties due to internal/external correlation change or baseline drift in respiration. However, re-modelling required additional exposures that were 8.3-16.7 times higher than intrafractional monitoring [4, 12]. Also, x-ray image-based DTT, another DTT approach with Vero4DRT [6], would not be an alternative strategy in terms of the difficulty of real-time detection and excessive imaging doses. In the current study, the overall mean errors of  $iE_P$  were calculated from around 30 paired images retrieved in the previous field using the monitoring function for the intrafractional tracking accuracy verification. Because the systematic prediction errors resulting from the baseline drift of respiration were reduced by subtracting the overall mean errors of  $iE_P$  in the previous field,  $iE_P^{95}$  decreased significantly in the CC and AP directions using the monitoring images during beam delivery. In the current study, we used all monitoring images to calculate the systematic prediction errors because  $iE_P$  varied according to the respiratory phase. However, a triggered x-ray acquisition based on the respiratory phase would also reduce  $iE_P^{95}$  using a small number of monitoring images because the systematic prediction errors could be corrected by the averaged  $iE_P$  at the end-expiratory and end-inspiratory phases.

## Intrafractional accuracy of IR Tracking

**CONCLUSIONS**

We demonstrated that IR Tracking reduced the impact of respiratory motion substantially. The prediction error was the primary cause of the overall targeting error, while the mechanical error was negligible. The PTV margin fully covered the intrafractional overall targeting errors. The 4D modelling errors during a dry-run treatment session were a good indicator of the prediction and overall targeting errors during the treatment course. Additionally, further improvement in prediction accuracy was achieved by correcting the systematic prediction error in the previous field.

**CONFLICTS OF INTEREST STATEMENT**

This research was sponsored in part by Mitsubishi Heavy Industries, Ltd., Japan. Takashi Mizowaki, Masaki Kokubo, and Masahiro Hiraoka have consultancy agreements with Mitsubishi Heavy Industries, Ltd.

**ACKNOWLEDGEMENTS**

This research was supported by the Japan Society for the Promotion of Science (JSPS) through its “Funding Program for World-Leading Innovative R&D on Science and Technology (FIRST Program).”

## REFERENCES

- [1] Keall P J, Mageras G S, Balter J M, *et al.* The management of respiratory motion in radiation oncology report of AAPM task group 76. *Med Phys* 2006;33:3874–900.
- [2] Korreman S S. Motion in radiotherapy: photon therapy. *Phys Med Biol* 2012;57:R161–91.
- [3] Matsuo Y, Shibuya K, Nakamura M, *et al.* Dose-volume metrics associated with radiation pneumonitis after stereotactic body radiation therapy for lung cancer. *Int J Radiat Oncol Biol Phys* 2012;83:e545–9.
- [4] Kamino Y, Takayama K, Kokubo M, *et al.* Development of a four-dimensional image-guided radiotherapy system with a gimbaled X-ray head. *Int J Radiat Oncol Biol Phys* 2006;66:271–8.
- [5] Takayama K, Mizowaki T, Kokubo M, *et al.* Initial validations for pursuing irradiation using a gimbals tracking system. *Radiother Oncol* 2009;93:45–9.
- [6] Mukumoto N, Nakamura M, Sawada A, *et al.* Positional accuracy of novel x-ray-image-based dynamic tumor-tracking irradiation using a gimbaled MV x-ray head of a Vero4DRT (MHI-TM2000). *Med Phys* 2012;39:6287–96.
- [7] Mukumoto N, Nakamura M, Sawada A, *et al.* Accuracy verification of infrared marker-based dynamic tumor-tracking irradiation using the gimbaled x-ray head of the Vero4DRT (MHI-TM2000). *Med Phys* 2013;40:041706-1–9.
- [8] Akimoto M, Nakamura M, Mukumoto N, *et al.* Predictive uncertainty in infrared marker-based dynamic tumor tracking with Vero4DRT. *Med Phys* 2013;40:091705-1–8.

## Intrafractional accuracy of IR Tracking

- 288 [9] Nakamura M, Mukumoto N, Ueki N, *et al.* Estimation of a tracking margin in  
289 surrogate signal-based dynamic tumor tracking irradiation with Vero4DRT. *Int J Radiat*  
290 *Oncol Biol Phys* 2012;84:S851–2.
- 291 [10] Matsuo Y, Sawada A, Ueki N, *et al.* An initial experience of dynamic tumor tracking  
292 irradiation with real-time monitoring using Vero4DRT (MHI-TM2000). *Radiother*  
293 *Oncol* 2012;103:S64.
- 294 [11] Depuydt T, Verellen D, Haas O, *et al.* Geometric accuracy of a novel gimbals based  
295 radiation therapy tumor tracking system. *Radiother Oncol* 2011;98:365-72.
- 296 [12] Depuydt T, Poelsa K, Verellen D, *et al.* Initial assessment of tumor tracking with a  
297 gimballed linac system in clinical circumstances: A patient simulation study. *Radiother*  
298 *Oncol* 2013;106:236–40.
- 299 [13] Ueki N, Matsuo Y, Nakamura M, *et al.* Intra- and interfractional variations in geometric  
300 arrangement between lung tumours and implanted markers. *Radiother Oncol* 2013, in  
301 press.
- 302 [14] Hoogeman M, Prévost J B, Nuytens J, *et al.* Clinical accuracy of the respiratory tumor  
303 tracking system of the cyberknife: assessment by analysis of log files. *Int J Radiat*  
304 *Oncol Biol Phys* 2009;74:297–303.
- 305 [15] Pepin E W, Wu H, Zhang Y, *et al.* Correlation and prediction uncertainties in the  
306 cyberknife synchrony respiratory tracking system. *Med Phys* 2011;38:4036-44.
- 307 [16] Malinowski K, McAvoy T J, George R, *et al.* Incidence of changes in  
308 respiration-induced tumor motion and its relationship with respiratory surrogates  
309 during individual treatment fractions. *Int J Radiat Oncol Biol Phys* 2012;82:1665–73.
- 310

## Intrafractional accuracy of IR Tracking

### FIGURE LEGENDS

**Figure 1.** Screen shot of the Vero4DRT during infrared (IR)-marker-based DTT irradiation (“IR Tracking”). Monitored fiducial markers’ positions were located outside of the “Tolerance circle” displayed around the predicted fiducial markers’ positions due to the baseline drift of respiration.

**Figure 2.** Probability histograms of positional errors in the cranio-caudal (CC) direction (a) for the first patient who underwent IR Tracking (Patient No. 1) and (b) for the most improved patient with intrafractional prediction error ( $iE_P$ ) correction (Patient No. 7). The Vero4DRT reduced the motion blurring effect caused by respiration.

## TABLES

**Table 1.** Characteristics of the patients and treatment planning.

Patient no.	Age (y.o.)	Sex	Tumour stage	Tumour side	Tumour location	A [mm]			$E_{4DM}^{\mu+2SD}$ [mm]			GTV [cc]	PTV margin [mm]			PTV [cc]
						LR	CC	AP	LR	CC	AP		LR	CC	AP	
1	85	F	Metastasis	Rt	S6	2.2	14.8	2.2	0.2	1.4	0.6	38.7	5.0	7.0	5.0	87.0
2	82	M	T1a	Rt	S9	4.6	19.8	4.4	1.6	3.3	0.5	11.0	5.0	8.0	5.0	34.6
3	86	F	T1b	Rt	S9	2.2	26.0	5.3	0.2	1.6	0.8	12.4	5.0	8.0	5.0	38.0
4	84	M	T1b	Rt	S6	0.9	11.9	3.1	0.3	1.3	0.7	17.8	5.0	7.0	5.0	50.1
5	71	M	T1b	Rt	S5	7.4	3.4	5.1	1.3	1.0	0.7	12.5	5.0	5.0	5.0	33.6
6	87	M	T1b	Lt	S8	2.9	29.6	15.5	0.6	2.2	3.9	20.6	5.0	8.0	8.0	64.1
7	61	M	T2a	Rt	S10	1.4	8.8	4.0	0.5	2.6	0.7	31.9	5.0	6.5	5.0	74.2
8	85	M	T1a	Lt	S9	5.8	30.6	8.7	2.1	3.4	2.9	8.9	5.0	9.0	6.0	33.4
9	68	M	Metastasis	Lt	S8	2.7	9.9	2.3	0.2	0.9	0.4	2.3	5.0	5.0	5.0	10.4
10	60	M	Metastasis	Rt	S9	3.1	16.7	4.1	0.9	2.2	1.6	13.3	5.0	7.0	5.0	38.9

Abbreviations: A=peak-to-peak amplitude of respiration,  $E_{4DM}^{\mu+2SD}$  = mean plus two standard deviations of the absolute 4D-modelling error during a dry-run treatment session, GTV=gross tumour volume, PTV=planning target volume, LR=left-right, CC=cranio-caudal, AP=anterior-posterior, F=Female, M=Male, Rt=Right lobe, Lt=Left lobe, S= pulmonary segment.

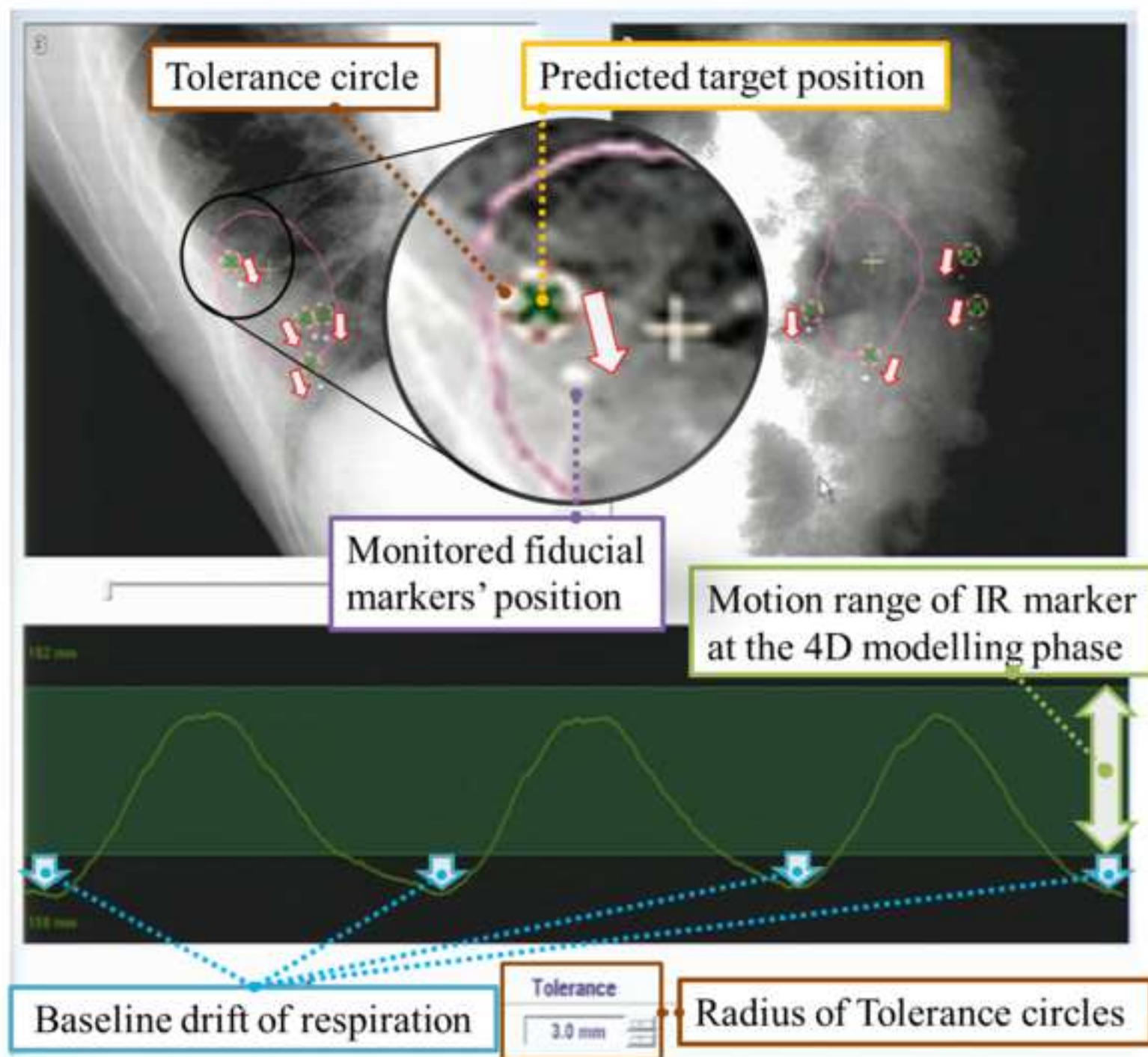
**Table 2.**  $iE_M^{95}$ ,  $iE_P^{95}$ ,  $iE_T^{95}$ , and corrected  $iE_P^{95}$ .

Patient no.	$iE_M^{95}$ [mm]			$iE_P^{95}$ [mm]			$iE_T^{95}$ [mm]			Corrected $iE_P^{95}$ [mm]		
	LR	CC	AP	LR	CC	AP	LR	CC	AP	LR	CC	AP
1	0.1	0.3	0.1	0.6	2.7	1.3	0.9	2.3	1.0	0.6	1.9	1.2
2	0.3	0.7	0.2	1.4	3.4	0.8	1.3	3.0	0.7	1.3	3.1	0.6
3	0.1	0.4	0.1	0.7	2.5	1.5	0.8	2.2	1.0	0.7	2.7	1.3
4	0.1	0.4	0.1	0.8	2.0	1.5	0.8	1.7	1.0	0.8	1.7	1.4
5	0.1	0.1	0.1	1.8	1.5	1.6	1.1	1.5	1.2	1.5	1.5	1.6
6	0.1	0.3	0.1	1.0	2.5	5.0	1.9	2.3	2.9	0.9	1.8	4.3
7	0.2	0.8	0.2	2.1	4.1	2.3	1.4	4.1	1.6	0.7	2.7	1.4
8	0.2	0.4	0.1	2.1	3.2	3.4	2.2	2.8	1.6	2.5	3.2	3.2
9	0.1	0.3	0.1	0.5	1.6	1.4	0.8	1.4	0.9	0.4	1.3	1.1
10	0.1	0.3	0.1	1.1	3.0	2.0	1.3	2.9	1.6	1.0	2.7	1.8
Average	0.1	0.4	0.1	1.2	2.7	2.1	1.3	2.4	1.4	1.0	2.3	1.8

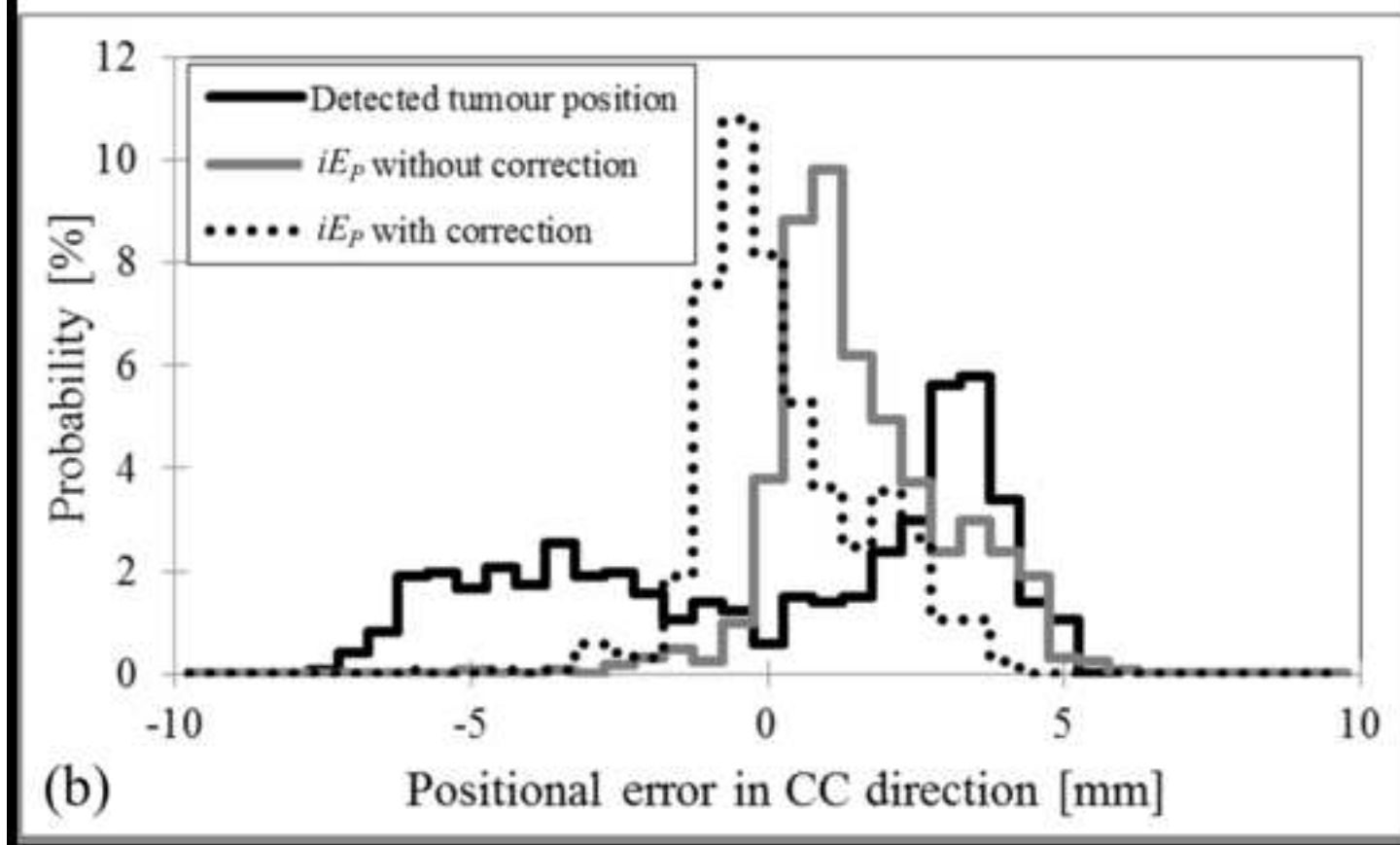
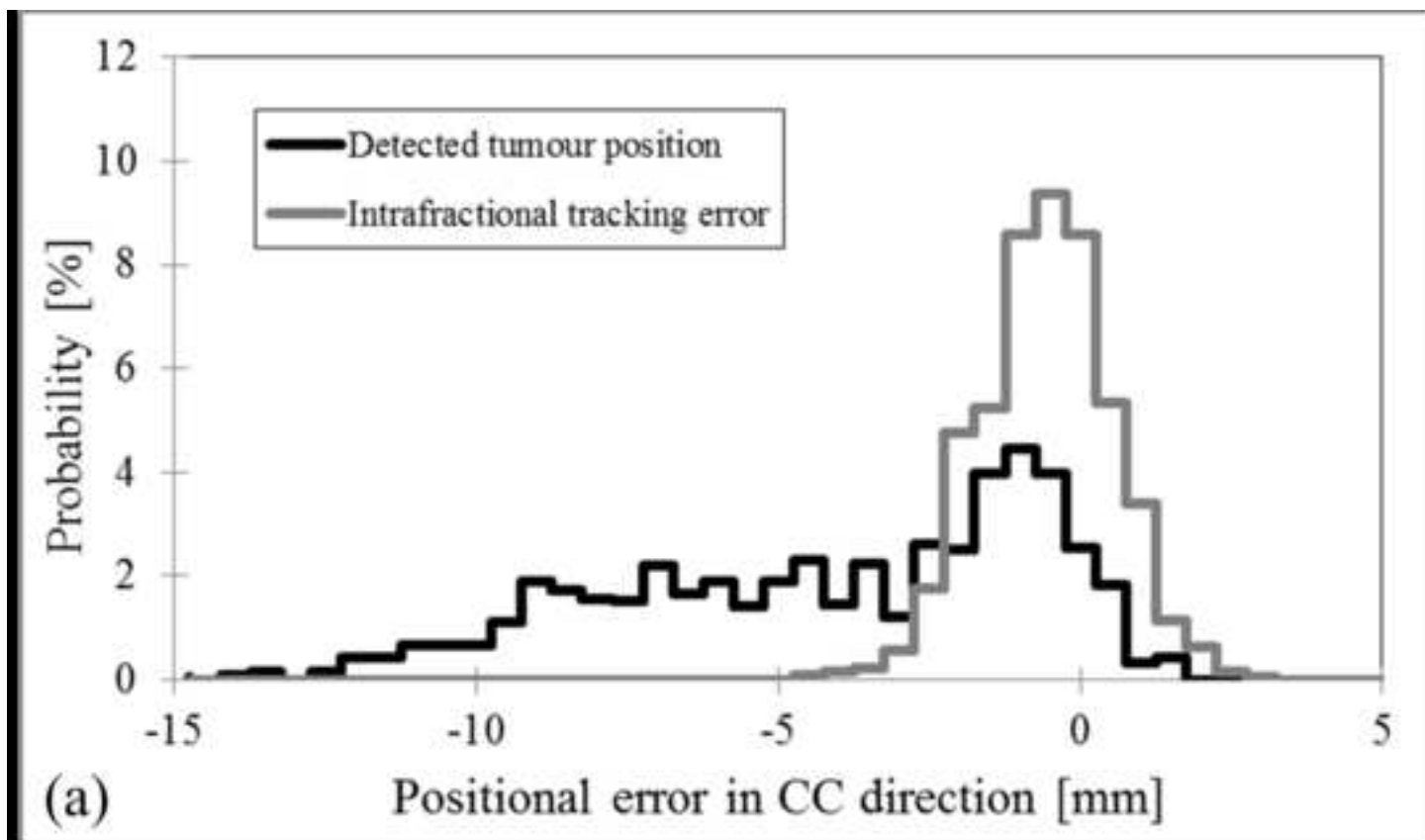
Abbreviations:  $iE_M^{95}$ =95<sup>th</sup> percentiles of the absolute intrafractional mechanical error,  $iE_P^{95}$ =95<sup>th</sup> percentiles of the absolute intrafractional prediction error,  $iE_T^{95}$ =95<sup>th</sup> percentiles of the absolute intrafractional overall targeting error, LR=left-right, CC=cranio-caudal, AP=anterior-posterior.

Figure 1

[Click here to download high resolution image](#)







# ***Prediction model of the Vero4DRT***

Before irradiation, a prediction model (“4D model”) was created. Infrared (IR) marker displacements and the implanted fiducial markers’ motions were monitored for 20-40 s using the IR camera of the ExacTRAC system every 16.7 ms and the orthogonal kV x-ray imaging subsystems every 80 or 160 ms, respectively. The frame rate of x-ray monitoring changed automatically depending on IR marker velocity.

After monitoring, two target positions are determined: the detected target position ( $P_d$ ) and the predicted target position ( $P_p$ ). The  $P_d$  is defined as the tumour centre-of-mass calculated from the positions of the implanted fiducial markers on the x-ray images. The relative shift amount between the tumour centre-of-mass and centroid of the markers’ polyhedron was determined at the end-exhalation phase in the planning computed tomography. The positions of the implanted fiducial markers were detected automatically based on the intensity ratios of the fiducial markers to their surroundings with an accuracy of 0.2 mm. The  $P_p$  is calculated from the predicted position and velocity of IR markers using the 4D model, expressed as follows:

$$P_p = \begin{pmatrix} x_p \\ y_p \\ z_p \end{pmatrix} = \frac{1}{n} \begin{pmatrix} \sum_{i=1}^n (a_{x,i}s_i^2 + b_{x,i}s_i + c_{x,i} + d_{x,i}v_i^2 + e_{x,i}v_i) \\ \sum_{i=1}^n (a_{y,i}s_i^2 + b_{y,i}s_i + c_{y,i} + d_{y,i}v_i^2 + e_{y,i}v_i) \\ \sum_{i=1}^n (a_{z,i}s_i^2 + b_{z,i}s_i + c_{z,i} + d_{z,i}v_i^2 + e_{z,i}v_i) \end{pmatrix} \quad (\text{equation1}),$$

where  $x_p$ ,  $y_p$ , and  $z_p$  are the predicted target positions in the left-right, cranio-caudal, and anterior-posterior directions,  $n$  is the number of IR markers, and  $s$  and  $v$  are the predicted position and velocity of each IR marker in the anterior-posterior direction. The positions of

## Mukumoto et al. Intrafractional accuracy of IR Tracking

20 the IR markers are predicted from the past motion to compensate for DTT system delay.  
21 Parameters of the 4D model ( $a$ ,  $b$ ,  $c$ ,  $d$ , and  $e$ ) were optimised using a least-squares  
22 algorithm so that residual errors between the  $P_p$  and  $P_d$  were minimised.

23 During beam delivery, the future 3D target position is predicted from the  
24 displacements of the IR markers using the 4D model, and then the corresponding tracking  
25 angle is transferred continuously to the gimballed x-ray head.

26

Mukumoto et al. Intrafractional accuracy of IR Tracking

27 ***Tracked target position calculated from the tracking angle of the gimballed x-ray head***

28 Intrafractional tracking accuracy was assessed by the detected target position ( $P_d$ ) from the  
29 fluoroscopic images and the corresponding predicted target position ( $P_p$ ) and the tracked  
30 target position, calculated from the synchronously acquired log files. The tracked target  
31 position was derived from an intersection of a tracking orientation of the gimballed x-ray  
32 head with a tracked tumour plane. The tracked tumour plane was defined as the  
33 perpendicular plane to the gimbal angle of  $0^\circ$  for each port at the depth of the moving  
34 tumour. The tracked target position, based on  $P_d$  ( $P_{t,d}$ ), was calculated in the following three  
35 steps:

36 (1) Conversion of  $P_d$  from room to gantry-ring coordinates:

$$37 \begin{pmatrix} u_d \\ v_d \\ w_d \end{pmatrix} = \begin{pmatrix} \cos G \cos R & -\cos G \sin R & -\sin G \\ -\sin R & -\cos R & 0 \\ \sin G \cos R & -\sin G \sin R & \cos G \end{pmatrix} \cdot \begin{pmatrix} x_d \\ y_d \\ z_d \end{pmatrix} \quad (\text{equation 2}),$$

38 where  $x_d$ ,  $y_d$ , and  $z_d$  are the detected target positions along the LR, the CC, and the AP  
39 directions in room coordinates, and  $G$  and  $R$  are the gantry and ring angle, and  $u_d$ ,  $v_d$ , and  
40  $w_d$  (units: mm) are the detected target positions in gantry-ring coordinates corresponding to  
41  $x_d$ ,  $y_d$ , and  $z_d$ .

42 (2) Calculation of  $P_{t,d}$  at the depth of  $P_d$  in gantry-ring coordinates

$$43 \begin{pmatrix} u_{t,d} \\ v_{t,d} \\ w_{t,d} \end{pmatrix} = \begin{pmatrix} (960 - w_d) \tan \theta_p \\ (960 - w_d) \tan \theta_r \\ w_d \end{pmatrix} \quad (\text{equation 3}),$$

44 where  $u_{t,d}$ ,  $v_{t,d}$ , and  $w_{t,d}$  (units: mm) are the tracked target positions in gantry-ring

# Mukumoto et al. Intrafractional accuracy of IR Tracking

coordinates at the depth of the detected target position ( $w_{t,d}$ ).  $\theta_p$  and  $\theta_T$  are the pan and tilt angle of the gimballed x-ray head, and 960 mm is the distance from the rotation centre of the gimballed x-ray head to the isocentre.

(3) Conversion of  $P_{t,d}$  from gantry-ring to room coordinates:

$$\begin{pmatrix} x_{t,d} \\ y_{t,d} \\ z_{t,d} \end{pmatrix} = \begin{pmatrix} \cos G \cos R & -\sin R & \sin G \cos R \\ -\cos G \sin R & -\cos R & -\sin G \sin R \\ -\sin G & 0 & \cos G \end{pmatrix} \begin{pmatrix} u_{t,d} \\ v_{t,d} \\ w_{t,d} \end{pmatrix} \quad (\text{equation 4}),$$

where  $x_{t,d}$ ,  $y_{t,d}$ , and  $z_{t,d}$  (units: mm) are the tracked target positions in room coordinates. The tracked target position, based on  $P_p$  ( $P_{t,p}$ ), at the depth of the predicted target position ( $w_p$ ) was calculated similarly.

Intrafractional mechanical ( $iE_M$ ), prediction ( $iE_P$ ), and overall targeting errors ( $iE_T$ ) were defined as follows:

$$iE_M = \begin{pmatrix} x_{t,p} \\ y_{t,p} \\ z_{t,p} \end{pmatrix} - \begin{pmatrix} x_p \\ y_p \\ z_p \end{pmatrix} \quad (\text{equation 5}),$$

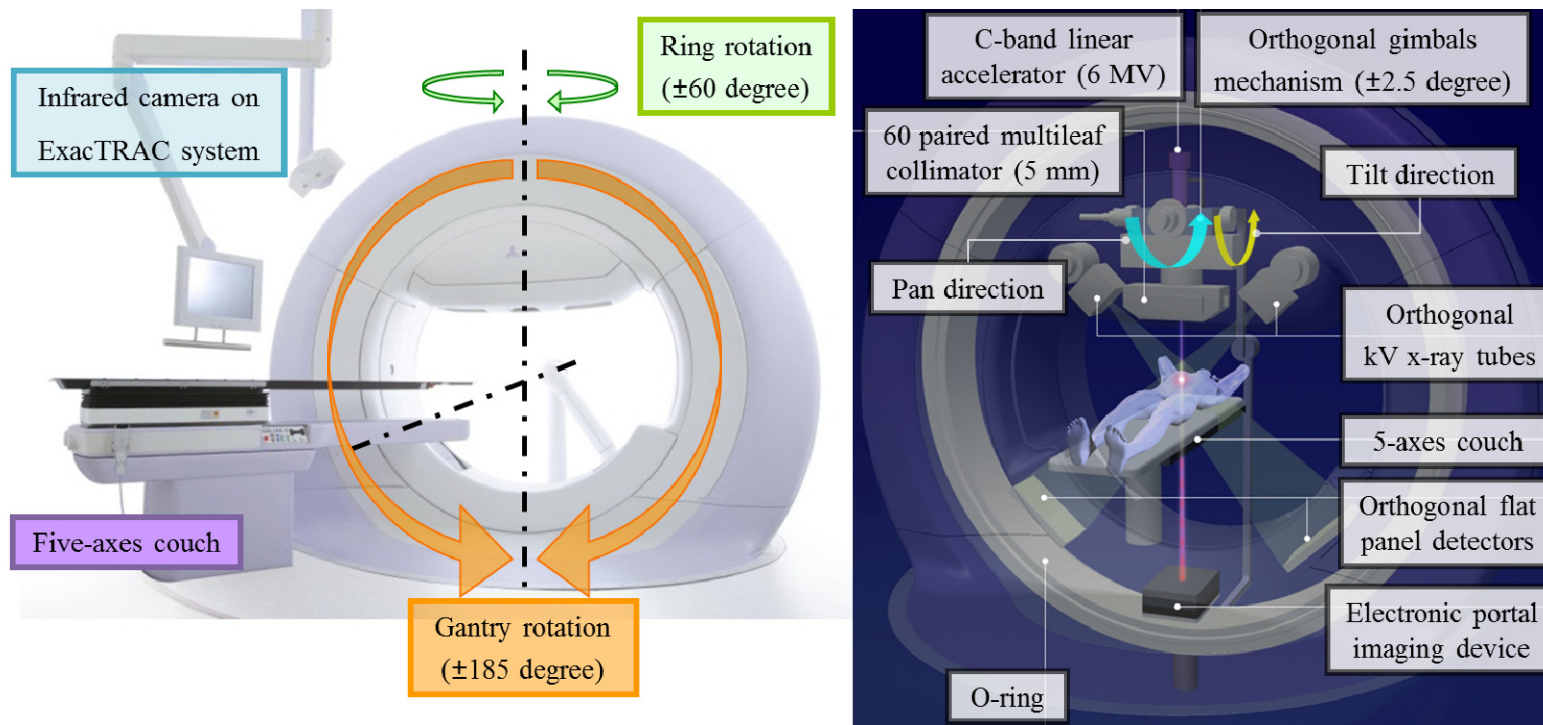
$$iE_P = \begin{pmatrix} x_p \\ y_p \\ z_p \end{pmatrix} - \begin{pmatrix} x_d \\ y_d \\ z_d \end{pmatrix} \quad (\text{equation 6}),$$

$$iE_T = \begin{pmatrix} x_{t,d} \\ y_{t,d} \\ z_{t,d} \end{pmatrix} - \begin{pmatrix} x_d \\ y_d \\ z_d \end{pmatrix} \quad (\text{equation 7}),$$

where  $x_{t,p}$ ,  $y_{t,p}$ , and  $z_{t,p}$  (units: mm) are the tracked target positions at the depth of the  $P_p$  used for the verification of the mechanical error of the gimballed x-ray head against the

## Mukumoto et al. Intrafractional accuracy of IR Tracking

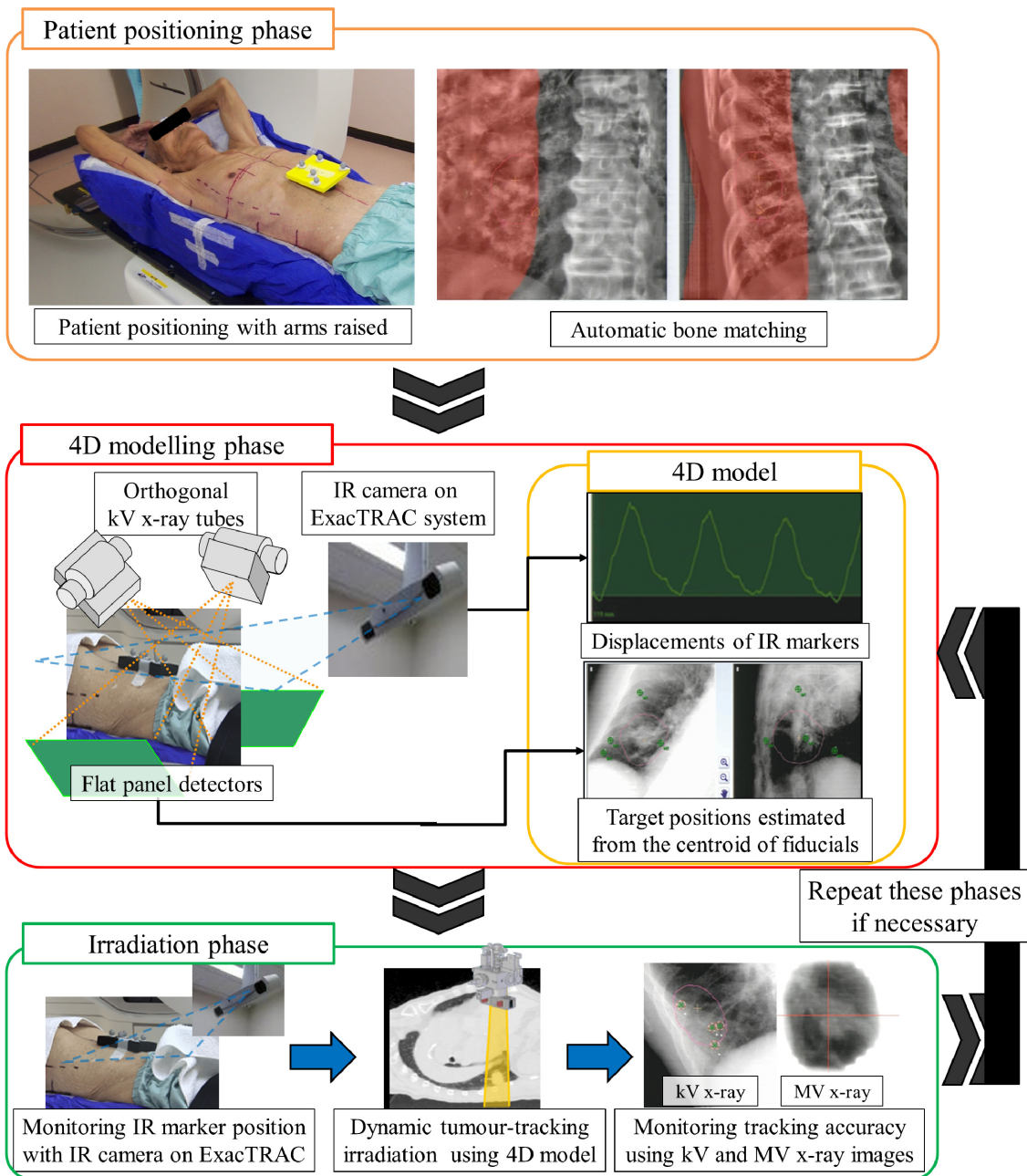
60 predicted target positions, and  $x_p$ ,  $y_p$ , and  $z_p$  (units: mm) are the predicted target positions  
61 used as the tracking commands to the gimballed x-ray head, and  $x_d$ ,  $y_d$ , and  $z_d$  (units: mm)  
62 are the detected target positions, and  $x_{t,d}$ ,  $y_{t,d}$ , and  $z_{t,d}$  (units: mm) are the tracked target  
63 positions at the depth of the  $P_d$  used for the verification of the overall targeting error of the  
64 gimballed x-ray head against the moving tumour.



65

66 **Supplementary Figure 1.** Schematic diagram of the Vero4DRT system.

Mukumoto et al. Intrafractional accuracy of IR Tracking



67

68 **Supplementary Figure 2.** Infrared (IR) marker-based hybrid dynamic tumour tracking

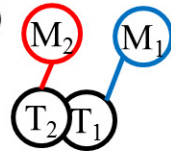
69 irradiation ("IR Tracking") procedure.



# Patient-specific PTV margin

## (1) Interfractional error

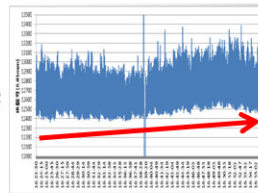
- Geometric uncertainty between Marker ( $M_n$ ) and Target ( $T_n$ )
  - 2.5 mm



## (2) Intrafractional error (Systematic)

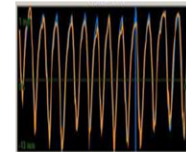
- Baseline drift of respiration
  - 10% of peak-to-peak Amplitude

Amplitude



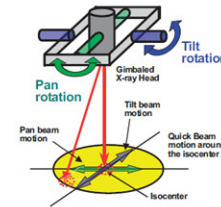
## (3) Intrafractional error (Random)

- 4D modelling error
  - Mean + 2SD of absolute 4D modelling error



## (4) Intrafractional error (Random)

- Mechanical error
  - 95<sup>th</sup> percentiles of mechanical error

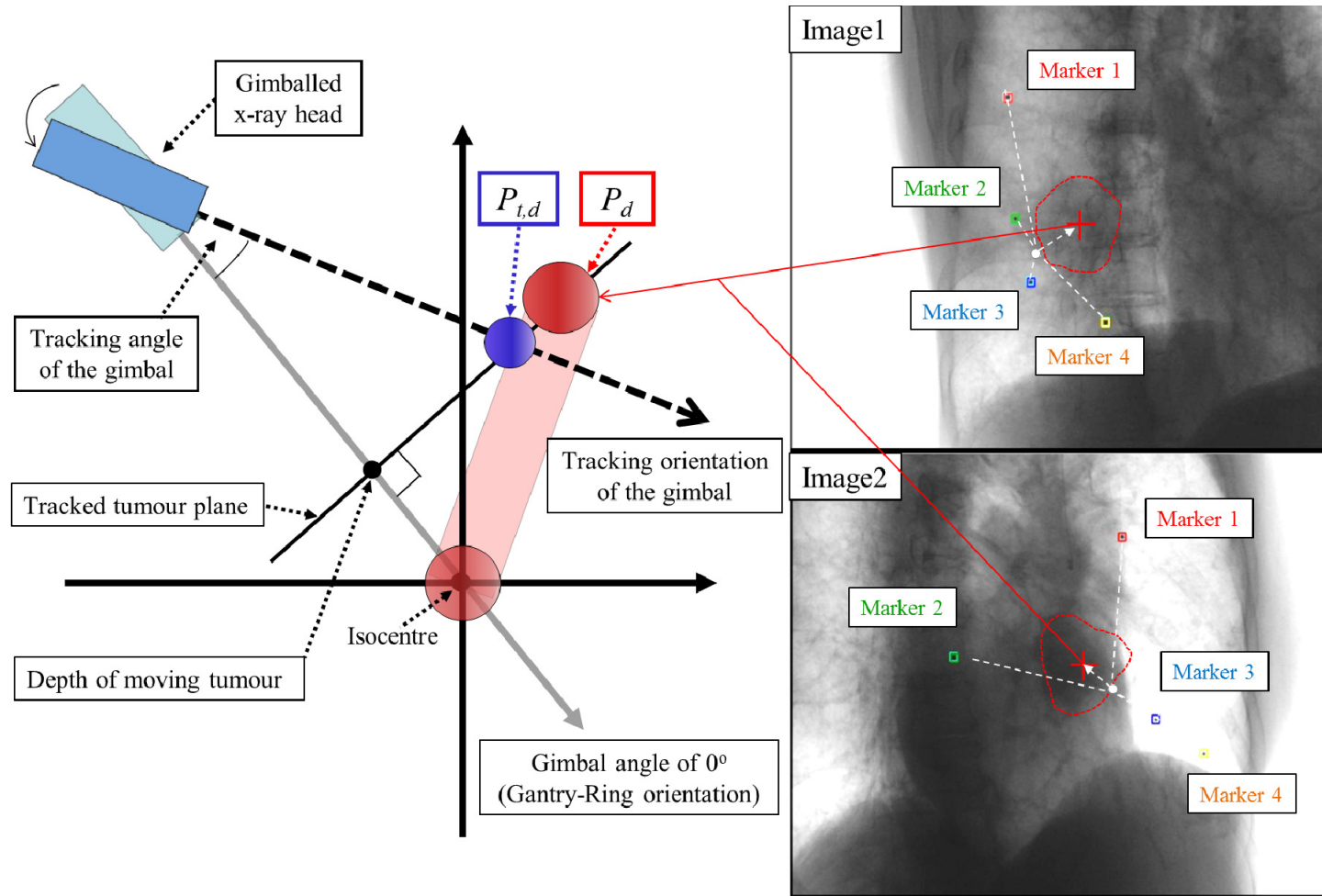


$$PTV \text{ margin [mm]} = (1) + (2) + \sqrt{(3)^2 + (4)^2}$$

**Minimum size of PTV margin was set to 5 mm**

70

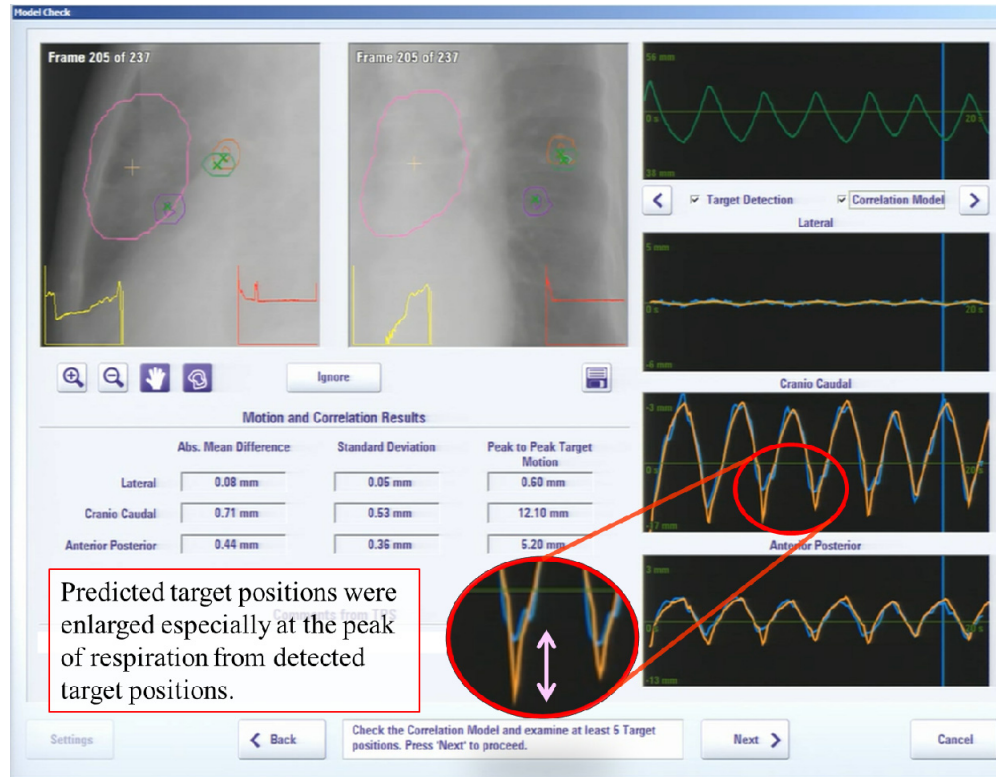
71 **Supplementary Figure 3.** Definition of the patient-specific planning target volume (PTV) margin.



72

73 **Supplementary Figure 4.** The geometric point of the tracked target position ( $P_{t,d}$ ) based on the detected target position ( $P_d$ )

74 calculated from orthogonal fluoroscopic images and synchronously acquired log files.



75

76 **Supplementary Figure 5.** Screen shot of the Vero4DRT system during creation of the prediction model (“4D model”). The

77 right four groups of waves, from top to bottom, show variations in the infrared (IR) markers’ positions in the

78 anterior-posterior direction and the target positions in the lateral, craniocaudal, and anterior-posterior directions, respectively.

79 In the graphs of the target position, dark-coloured waves show the detected target position and light-coloured waves show the

80 predicted target position.